

Article

Time-Dependent Stagnation Point Flow of Water Conveying Titanium Dioxide Nanoparticle Aggregation on Rotating Sphere Object Experiencing Thermophoresis Particle Deposition Effects

Javali K. Madhukesh ¹, Ballajja C. Prasannakumara ¹, Umair Khan ^{2,3,*}, Sunitha Madireddy ⁴, Zehba Raizah ⁵ and Ahmed M. Galal ^{6,7}

¹ Department of Studies and Research in Mathematics, Davangere University, Davangere 577002, Karnataka, India; madhukeshjk@gmail.com (J.K.M.); dr.bcprasanna@gmail.com (B.C.P.)

² Department of Mathematical Sciences, Faculty of Science and Technology, Universiti Kebangsaan Malaysia, Bangi 43600, Selangor, Malaysia

³ Department of Mathematics and Social Sciences, Sukkur IBA University, Sukkur 65200, Sindh, Pakistan

⁴ Department of Mathematics and Statistics, University College for Women, Koti 500095, Hyderabad, India; sunithareddy133@gmail.com

⁵ Department of Mathematics, College of Science, King Khalid University, Abha 61421, Saudi Arabia; zaalrazh@kku.edu.sa

⁶ Mechanical Engineering Department, College of Engineering, Prince Sattam Bin Abdulaziz University, Wadi Addawaser 11991, Saudi Arabia; ahm.mohamed@psau.edu.sa

⁷ Production Engineering and Mechanical Design Department, Faculty of Engineering, Mansoura University, Mansoura P.O. Box 35516, Egypt

* Correspondence: umairkhan@iba-suk.edu.pk



Citation: Madhukesh, J.K.; Prasannakumara, B.C.; Khan, U.; Madireddy, S.; Raizah, Z.; Galal, A.M.

Time-Dependent Stagnation Point Flow of Water Conveying Titanium Dioxide Nanoparticle Aggregation on Rotating Sphere Object Experiencing Thermophoresis Particle Deposition Effects. *Energies* **2022**, *15*, 4424. <https://doi.org/10.3390/en15124424>

Academic Editor: Gianpiero Colangelo

Received: 19 May 2022

Accepted: 15 June 2022

Published: 17 June 2022

Publisher's Note: MDPI stays neutral with regard to jurisdictional claims in published maps and institutional affiliations.



Copyright: © 2022 by the authors. Licensee MDPI, Basel, Switzerland. This article is an open access article distributed under the terms and conditions of the Creative Commons Attribution (CC BY) license (<https://creativecommons.org/licenses/by/4.0/>).

Abstract: The notion of thermophoretic particle deposition is used in a number of applications, including thermal exchanger walls. It is important to identify the transport processes in action in systems such as thermal precipitators, exhaust devices, optical transmission fabrication processes, and so on. Based on these application points of view, the present work studies the performance of nanoparticle aggregation stagnation point flow over a rotating sphere during the occurrence of thermophoretic particle deposition. The nonlinear governing equations are transformed into the ordinary differential equation by utilizing suitable similarity variables. The numerical outcomes of the reduced equations along with boundary conditions are solved by the Runge–Kutta–Fehlberg 45 (RK45) order method with shooting procedure. The numerical results are shown with the assistance of graphs. The impacts of various dimensionless constraints on velocity, thermal, and concentration profiles are studied under the occurrence and absence of nanoparticle aggregation. The study reveals that the primary velocity is enhanced with increasing values of the acceleration parameter, but secondary velocity diminishes. The impressions of the rotation parameter will improve the primary velocity. The concentration profiles will diminish with an improvement in the thermophoretic parameter. The surface drag force is greater in nanoparticles with aggregation than nanoparticles without aggregation in the C_{fx} case but a reverse behavior is seen in the C_{fz} case. Further, the rate of heat distribution increases with a rise in the solid volume fraction, whereas the rate of mass distribution grows as the thermophoretic parameter grows.

Keywords: nanofluid; nanofluid aggregation; thermophoretic particle deposition; stagnation point flow; rotating sphere

1. Introduction

Nanofluids are a new category of nanotechnology-based thermal transfer liquids that are created by dissolving and suspending nanosized particles with distinctive diameters on

the order of 10 nanometers. Base liquids often include water, motor oil, organic liquids, and other basic liquids. Choi [1] hypothesized about the possession of thermal conductivity and thermal transfer using nanofluids in 1995. A nanofluid is a developing liquid that has resulted in a number of scientific achievements in the nano industry. Choi, in his survey, discovered that a nanofluid is more efficient than any other fluid. The majority of nanofluid articles focus on understanding their behavior so that they may be used in situations where direct heat transfer improvement is critical, such as in many industrial applications, nuclear reactors, transportation, electronics, medicine, and food. Recently, in the context of a Casson nanofluid, Abu et al. [2] conducted a theoretical examination of a single vapor bubble in power-law fluid impacted by varying surface tension over $\text{Al}_2\text{O}_3/\text{H}_2\text{O}$ nanofluids. Prasannakumara [3] used NaAlg-Cu nanofluid to conduct a quantitative investigation of the local thermal non-equilibrium conditions for a nano liquid (NaAlg-Cu) passing over a porous medium. Khan et al. [4] investigated the Cattaneo–Christov thermal flow model and the OHAM approach across three distinct fluids. The study demonstrated that a progressive increase in thermal relaxation parameters results in fluid temperature exhaustion and an increased heat transfer rate. Alzahrani et al. [5] explored the influence of thermal radiation with suction and slip conditions in the presence of a Casson nanofluid over a plane wall jet. Morad et al. [6] examined the thermophysical bubble movements in an N-dimensional $\text{Al}_2\text{O}_3/\text{H}_2\text{O}$ nano liquid under two-phase turbulent flow. Bhowmik et al. [7] conducted a rod bundle thermal–hydraulic investigation with water and a water-based Al_2O_3 nanofluid for a tiny compact reactor. Computational assessment of the thermo-hydraulic performance of an Al_2O_3 –water-based nanofluid in a hexagonal rod-bundle sub-channel was explored by Ahmed et al. [8].

When a group of nanoparticles stick together, they combine to form nanoparticle aggregation (N-Ag). The decrease in the contact surface of the fluid–solid interfaces results in a drop in the potential energy of the fluid system. Viscosity and thermal conductivity directly impact N-Ag. The aggregated nanoparticles tend to build flowing networks and continuous links to create a reduced thermal pathway. As a result, heat may be conveyed rather rapidly across the groupings, which, when combined with the augmented aggregation volume compared to nanoparticles, can increase the thermal capacity of the nanofluid. Thermal conductivity enhancement by the aggregation of nanoparticles with the occurrence of metal oxides and nanoparticles was studied by Wensel et al. [9]. Based on the nanolayer and nanoparticle aggregation, Xie et al. [10] determined the effective thermal conductivity of nanofluids. Swain and Mahanthesh et al. [11] investigated the N-Ag and Joule heating effect in a radiating magneto nano liquid flow over an exponential area. Rana et al. [12] inspected the Cattaneo–Christov (C-C) model and heat flux effects on a spinning disk with the Hall current effect in the presence of N-Ag. With sensitivity analysis, Sabu et al. [13] studied N-Ag dynamics on the quadratic convective magnetohydrodynamic flow of a nanomaterial across a slanted flat plate. Regarding the flow of a micropolar nanofluid across a stretching surface, Yu et al. [14] explored N-Ag and the thermophoretic particle deposition process. Radiative heat transmission and unsteady movement in an uneven channel with the aggregation kinematics of a nanofluid were explored by Jestine and Mahanthesh [15]. The aspects of a uniform horizontal magnetic field and N-Ag in the flow of a nanofluid with melting heat transfer were explored by Wang et al. [16].

When particles in a gas move from hot to cold zones as a result of a temperature profile, this is known as thermophoretic particle deposition (T-P-D). Settlement on cold surfaces, such as heat exchanger walls, might be aided by this movement. It is vital to understand the transport mechanisms at work in systems such as exhaust systems and thermal precipitators, and optical waveguide production procedures are critical. The practical application of the present concept was explained by Green and Lane [17] and Fuchs [18]. T-P-D was first studied by Goren [19]. Recently, Madhukesh et al. [20] inspected the mass and thermal transfer during the occurrence of a Casson fluid containing hybrid nanoparticles over a Riga surface in the context of the T-P-D effect. Waini et al. [21] investigated T-P-D and viscous dissipation effects in a micropolar hybrid nanofluid over a flat surface. Shankaralin-

gappa et al. [22] investigated the T-P-D on a three-dimensional flow of Casson nano liquid containing sodium alginate across a stretched surface. Chen et al. [23] investigated T-P-D in the flow of a dual-layer Casson liquid with a magnetic dipole and extended Fourier's and Fick's equations. Madhukesh et al. [24] considered the thermophoretic impact and convective thermal conditions on the flow of a hybrid nanofluid over a moving thin needle. Gowda et al. [25] explored thermal transport in ferromagnetic liquid dynamics across a stretched sheet with the combined effects of T-P-D and a magnetic dipole.

Because all fluid flow and solid structure relationships are linked to stagnation point flow performance, stagnation point flow is a significant phenomenon. In engineering applications, the rate of fluctuation of the physical limitations around the flow is critical. The pressure and largest thermal exchange, as well as a reduction in velocity, occur near the flow's environments in stagnation point motion. Electronic, hydrodynamic, and aerodynamic fields all play essential roles in flow at the stagnation point. The phenomenon of flow at the stagnation point has several applications in fluid flow and thermal transmission in a number of industries and technical domains. Zaib et al. [26] explored the creation of entropy and the dual branch solution in a mixed convection stagnation point flow over a Riga surface in the context of a micropolar nanofluid flow. Khan et al. [27] scrutinized the flow at the stagnation point in the presence of a hybrid nano liquid along a non-isothermal shrinking/stretching sheet with inertial and microstructure features. Gul et al. [28] explored the stagnation point flow of a blood-based hybrid nanofluid under mixed convection around a revolving sphere. Ghasemi and Hatami [29] investigated how solar radiation affects MHD stagnation point flow and heat conduction in a nanofluid over a stretched sheet.

The rotational flows and heat transfer properties of a driven flow stream over stationary spinning bodies of revolution are essential in a number of engineering applications, such as ballistic re-entry, fiber coatings, projectile motion, and rotational equipment design. The heat distribution between a fluid flow and a revolving sphere has several applications in technology, such as overcoming freezing system difficulties. Malvandi [30] examined the time-dependent flow of an unsteady spinning sphere's stagnation point zone. Entropy analysis and unsteady MHD mixed convection stagnation point flow of a Casson nanofluid around a spinning sphere were examined by Madhy et al. [31]. Ahmed and Rashed [32] examined unsteady MHD mixed convection flow with the slip effect in a nanofluid in the stagnation region of an impulsively rotating sphere with the effects of thermal radiation and convective boundary conditions.

The present study was conducted to explore the behavior of nanoparticle aggregation and stagnation point flow over a rotating sphere in the presence of thermophoretic particle deposition.

The current study seeks to answer the following questions:

1. What is the impact of the nanoparticle aggregation effect on the acceleration parameter in velocity, thermal, and concentration profiles?
2. What is the thermal performance in the presence/absence of nanoparticle aggregation?
3. What is the impact of the thermophoretic effect on the concentration profile in the presence/absence of nanoparticle aggregation?

The present manuscript is divided into five sections. The context of the study and implementation is discussed in the Section 1. Section 2 expands on the modeling and formulation of the problem. Section 3 describes the numerical technique and validation of the code. Section 4 delineates the results and physical perspectives of the problem. Section 5 summarizes the outcomes of the study.

2. Materials and Methods

Consider the incompressible boundary layer unsteady movement of nanoparticles towards the forward stagnation point section at a persistent temperature on a rotating sphere, as in Figure 1. The x_1 coordinate is represented on the surface, and the direction normal to the sphere is denoted by y_1 . The sphere is rotating with angular velocity (time-dependent) $\Omega(t) = Bt^{-1}$, $B > 0$. The temperature near the wall is assumed to be constant. Furthermore,

The below similarity parameters are introduced (see [30]):

$$r_1 \approx x_1, \quad \frac{dr_1}{dx_1} = 1, \quad \eta = \frac{1}{\sqrt{\nu_f t}} y_1, \quad w_1 = \frac{Bx_1}{t} s(\eta) \tag{8}$$

$$\psi = Ax_1 \left(\frac{\nu_f}{t}\right)^{1/2} f(\eta), \quad \theta(\eta) = \frac{T_1 - T_\infty}{T_w - T_\infty}, \quad \chi(\eta) = \frac{C_1 - C_\infty}{C_w - C_\infty}$$

The thermophoretic velocity is represented as $V_T = -\frac{\nu_f K_{1a}^*}{T_{r1}} \frac{\partial T_1}{\partial y_1}$ (see [24]), where K_{1a}^* and T_{r1} are the thermophoretic constant and reference temperature, respectively.

According to experimental and empirical investigations (see [30–32]), in the kinematics and thermal propagation of nanofluid movements, the nanoparticle aggregation factor is critical. The nanomaterial measurement findings agreed exactly when the aggregate component was considered. The nanoparticle volume fraction is determined by the aggregation kinetic factor, and it is given as

$$\phi_{a2} = \phi \left(\frac{r_{a2}}{r_{p2}}\right)^{3-D_2} \tag{9}$$

As shown in Table 1 (see [33]), the thermal conductivity is determined by mixing the modified Maxwell and Bruggeman models. Suitable expressions are given below (see [34–36]).

$$\frac{k_{a2}}{k_f} = \frac{2}{8} \left\{ \frac{k_{p1}}{k_f} (3\phi_{i2} - 1) + (3(1 - \phi_{i2}) - 1) + \left[\left(\frac{k_{p2}}{k_f} (3\phi_{i2} - 1) + (3(1 - \phi_{i2}) - 1)\right)^2 + 8\frac{k_{p2}}{k_f} \right]^{0.5} \right\}$$

$$\phi_{i2} = \left(\frac{r_{a2}}{r_{p2}}\right)^{D_2-3}$$

$$\rho_{a2} = (1 - \phi_{i2})\rho_f + \phi_{i2}\rho_s,$$

$$(\rho C_p)_{a2} = (1 - \phi_{i2})(\rho C_p)_f + \phi_{i2}(\rho C_p)_s.$$

Table 1. Thermophysical properties of nanomaterials.

	Properties	Expression for Nanofluid
01	Viscosity	$\mu_{nf} = \mu_f \left(1 - \frac{\phi_{a2}}{\phi_{m2}}\right)^{-2.5\phi_{m2}}$
02	Density	$\rho_{nf} = \rho_f (1 - \phi_{a2}) + \phi_{a2} \frac{\rho_{a2}}{\rho_f}$
03	Heat capacity	$\frac{(\rho C_p)_{nf}}{(\rho C_p)_f} = \phi_{a2} \left(\frac{(\rho C_p)_{a2}}{(\rho C_p)_f}\right) + (1 - \phi_{a2})$
04	Thermal conductivity	$\frac{k_{nf}}{k_f} = \frac{2k_f + k_{a2} + 2\phi_{a2}(k_{a2} - k_f)}{2k_f + k_{a2} - \phi_{a2}(k_{a2} - k_f)}$

From the above-stated expressions, the subscripts $a2$ and $p2$ signify aggregates and nanoparticles, $\phi_{m2} = 0.605$ denotes particles that are spherical in shape, fractional index $D_2 = 1.8$, $r_{a2} = 3.34r_{p2}$ denotes the ratio of radii of aggregates to radii of nanoparticles and are the commonly accepted values.

By using Equation (8), the system of Equations (1)–(5) reduces and boundary conditions are transformed into:

$$f''' + A_1 A_2 \left[f' - A(f')^2 + f'' \left(\frac{\eta}{2} + fA\right) + A(\lambda s^2 + 1) - 1 \right] = 0 \tag{10}$$

$$s'' + A_1 A_2 \left[s(1 - 2Af') + s' \left(\frac{\eta}{2} + fA\right) \right] = 0 \tag{11}$$

$$\left(\frac{k_{nf}}{k_f}\right) \frac{\theta''}{A_3} + Pr\theta' \left[\frac{\eta}{2} + fA\right] = 0 \tag{12}$$

$$\chi'' + Sc \chi' \left[\frac{\eta}{2} + fA\right] - \tau_1 Sc(\chi\theta'' + \chi'\theta') = 0 \tag{13}$$

and

$$\begin{aligned} \text{at } \eta = 0: & \quad f = 0, \quad f' = 0, \quad \theta = 1, \quad \chi = 1, \quad s = 1 \\ \text{as } \eta \rightarrow \infty: & \quad f' = 1, \quad \theta = 0, \quad \chi = 0, \quad s = 0 \end{aligned} \tag{14}$$

The above Equations (10)–(14) comprised different controlling parameters which are defined namely and mathematically in Table 2.

Table 2. Flow controlling parameters.

	Name of the Parameter	Notation
01	Acceleration parameter	A
02	Rotation parameter	$\lambda = \frac{B^2}{A^2}$
03	Prandtl number	$Pr = \frac{\mu_f C_p}{k_f}$
04	Schmidt number	$Sc = \frac{\nu_f}{D_B}$
05	Thermophoretic parameter	$\tau_1 = -K_{1a}^*(T_w - T_\infty)T_{r1}^{-1}$
06		$A_1 = \left(1 - \frac{\phi_{a2}}{\phi_{m2}}\right)^{2.5\phi_{m2}}$
07		$A_2 = \left((1 - \phi_{a2}) + \left(\phi_{a2} \frac{\rho_{a2}}{\rho_f}\right)\right)$
08		$A_3 = \left(\phi_{a2} \left(\frac{(\rho C_p)_{a2}}{(\rho C_p)_f}\right) + (1 - \phi_{a2})\right)$

The important engineering coefficients C_{fx} , C_{fz} , Nu and Sh which are defined and simplified in Table 3. (see [30–32]).

Table 3. Engineering coefficients and its reduced form.

	Engineering Coefficients	Definition	Reduced Form
01	Surface drag forceIn x-direction	$C_{fx} = \frac{\mu_{nf} \left(\frac{\partial u}{\partial y}\right) \Big _{y=0}}{\rho_f u_e^2}$	$\sqrt{Re} C_{fx} = \frac{f''(0)a^{-\frac{1}{2}}}{A_1}$
02	Surface drag forceIn z-direction	$C_{fz} = -\frac{\mu_{nf} \left(\frac{\partial v_1}{\partial y}\right) \Big _{y=0}}{\rho_f u_e^2}$	$\sqrt{Re} C_{fz} = -\frac{a^{-\frac{1}{2}} \sqrt{\lambda} s'(0)}{A_1}$
03	Nusselt number	$Nu = \frac{-K_{nf} x \left(\frac{\partial T}{\partial y}\right) \Big _{y=0}}{K_f (T_w - T_\infty)}$	$\frac{Nu}{\sqrt{Re}} = -\frac{K_{nf}}{K_f} \frac{\theta'(0)}{\sqrt{a}}$
04	Sherwood number	$Sh = -\frac{x \left(\frac{\partial C_1}{\partial y}\right) \Big _{y=0}}{(C_{w1} - C_\infty)}$	$\frac{Sh}{\sqrt{Re}} = -x'(0) \sqrt{a}$

Where $Re = \frac{u_e x}{\nu_f}$ as the local Reynolds number.

3. Numerical Technique and Validation of the Code

The shooting methodology and RKF-45 method were utilized to find the solution of the reduced Equations (10)–(13) and boundary conditions (14) using well-known computational tools. The simplified equations are then transferred into a first-order system. Let us consider

$$\begin{aligned} f &= a_1, f' = a_2, f'' = a_3, \\ s &= a_4, s' = a_5, \\ \theta &= a_6, \theta' = a_7, \\ \chi &= a_8, \chi' = a_9 \end{aligned}$$

As a result, we obtain

$$a_3' = -A_1A_2 \left[(a_2 - Aa_2^2) + a_3 \left(\frac{\eta}{2} + a_1A \right) + A(\lambda a_4^2 + 1) - 1 \right] \tag{15}$$

$$a_5' = -A_1A_2 \left[a_4(1 - 2Aa_2) + a_5 \left(\frac{\eta}{2} + a_1A \right) \right] \tag{16}$$

$$a_7' = -\frac{A_3Prk_f}{k_{nf}} a_7 \left(\frac{\eta}{2} + a_1A \right) \tag{17}$$

$$a_9' = -Sc \left[a_9 \left(\frac{\eta}{2} + a_1A \right) - \tau_1 (a_7^1 a_8 + a_9 a_7) \right] \tag{18}$$

and

$$\left. \begin{aligned} f(0) = 0, f'(0) = 0, f''(0) = \delta_1, \\ S = 1, S' = \delta_2, \\ \theta = 1, \theta' = \delta_3, \\ \chi = 1, \chi' = \delta_4. \end{aligned} \right\} \tag{19}$$

The translated Equations (15)–(18) are numerically solved by estimating the missing boundary conditions as in Equation (19), using the shooting strategy and selecting the suitable value range for parameters as $A = \lambda = 1, Sc = 0.8, \tau_1 = 0.1$. The step size is set at 0.1, and the error tolerance is around 10^{-8} . The present numerical scheme is validated with the existing literature, it is found that the results are best matched with the work of [30]; moreover, the error percentage is calculated with the work of [30].

4. Results and Discussion

The effect of different dimensionless restrictions that control the flow, temperature and concentration characteristics across a spinning sphere in the presence of a TiO_2/H_2O -based nanofluid is discussed in this section. For all limitations, the investigation is performed in the presence/absence of nanoparticle aggregation. The numerical results are graphically illustrated to demonstrate how the individual dimensionless parameters (A, λ, Sc and τ_1) vary on the primary velocity, secondary velocity, temperature and concentration profiles. Table 1 shows the thermophysical characteristics of the nanomaterials. Table 2 displays the flow controlling parameters. The important engineering coefficients and its reduced form are tabulated in Table 3. The thermophysical characteristics of the base liquid and nanoparticles are shown in Table 4. The acquired numerical findings are compared to previously published literature (see Tables 5–7). The important engineering factors, such as C_{fx}, C_{fz}, Nu and Sh , are calculated for various constraints in the presence and absence of the nanoparticle aggregation, as shown in Tables 8 and 9.

Table 4. Thermophysical properties of base liquid and nanoparticles.

	ρ (Kg/m ³)	C_p (JK ⁻¹ kg ⁻¹)	k (Wm ⁻¹ K ⁻¹)	Pr
TiO ₂	4250	686.2	8.9538	-
H ₂ O	997.1	4179	0.613	6.2

Table 5. Comparison of $f''(0)$ for several values of A in the absence of ϕ .

	Ref. [37]	Ref. [30]	Present Result	Error %
	Quasilinearization	RK-4	RKF-45	
A	$f''(0)$	$f''(0)$	$f''(0)$	
0.5	0.79946	0.79913	0.79919	0.0075
1	1.28271	1.2828	1.28231	0.0389
2	1.91728	1.9172	1.91765	0.0234

Table 6. Comparison of $-s'(0)$ for several values of A in the absence of ϕ .

	Ref. [37]	Ref. [30]	Present Result	Error %
	Quasilinearization	RK-4	RKF-45	
A	$-s'(0)$	$-s'(0)$	$-s'(0)$	
0.5	0.30351	0.30339	0.30348	0.0296
1	0.64575	0.64579	0.64585	0.0092
2	1.05422	1.05415	1.05427	0.0113

Table 7. Comparison of $-\theta'(0)$ for several values of A in the absence of ϕ .

	Ref. [37]	Ref. [30]	Present Result	Error %
	Quasilinearization	RK-4	RKF-45	
A	$-\theta'(0)$	$-\theta'(0)$	$-\theta'(0)$	
0.5	0.46743	0.467648	0.467656	0.0017
1	0.58957	0.589527	0.589536	0.0015
2	0.77954	0.779526	0.779538	0.0015

Figures 2–5 display the influence of the acceleration parameter (A) on the primary velocity profile f' , secondary velocity profile s , temperature profile θ and concentration profile χ . Figure 2 shows that an inclination in the values of A will increase the primary velocity f' . The reverse trend is observed in the secondary velocity profile s (see Figure 3). With the rise in the value of A , the u_e also rises, which reduces the thickness of the boundary layer and increases the velocity in the lateral axis within the boundary layer. As a consequence, thermal distribution is decreased with a rise in A (see Figure 4). An increase in the values of A will diminish the thermal distribution due to a decrease in the thickness of the boundary layer. Similar behavior is exhibited by the concentration profile (see Figure 5). The velocity of the nanofluid with aggregation is lower when compared to nanoparticles without aggregation in the primary and secondary velocity profiles. Thermal dispersal is greater in the case of nanoparticles without aggregation than nanoparticles with aggregation. A similar trend is detected in the concentration profile.

Table 8. Computational values of C_{fx} , C_{fz} , Nu and Sh for various dimensionless constraints in the presence of nanoparticle aggregation with $\phi = 0.01$.

λ	Sc	τ_1	A	C_{fx}	C_{fz}	Nu	Sh
1	0.8	0.1	1	2.139808422	1.672304816	9.096392022	1.953593148
2				2.388841158	2.399686127	9.109856260	1.960978126
3				2.631209992	2.978918454	9.122719148	1.967982378
	0.8			2.139808422	1.672304816	9.096392022	0.511508126
	1.0			2.139808462	1.672304845	9.096392167	2.375204360
	1.2			2.139808462	1.672304845	9.096392167	2.796341524
		0.1		2.139808422	1.672304816	9.096392022	1.953593148
		0.3		2.139808462	1.672304845	9.096392167	2.971849166
		0.6		2.139808462	1.672304845	9.096392167	4.506727245
			0.5	1.136239692	0.897164782	8.985929840	1.846421159
			1.0	2.139808122	1.672304555	9.096391165	1.953593043
			1.5	3.091232933	2.389139595	9.212597417	2.049708182

Table 9. Computational values of C_{fx} , C_{fz} , Nu and Sh for various dimensionless constraints in the absence of nanoparticle aggregation with $\phi = 0.01$.

λ	Sc	τ_1	A	C_{fx}	C_{fz}	Nu	Sh
1	0.8	0.1	1	2.150493768	1.707536159	9.346671153	2.106243350
2				2.386049271	2.445904509	9.356523653	2.112991274
3				2.615895707	3.031585469	9.365992932	2.119423484
	0.8			2.150493768	1.707536159	9.346671153	2.106243350
	1.0			2.150493746	1.707536179	9.346671124	2.564734427
	1.2			2.150493746	1.707536179	9.346671124	3.022504984
		0.1		2.150493768	1.707536159	9.346671153	2.106243350
		0.3		2.150493746	1.707536179	9.346671124	3.414321918
		0.6		2.150493746	1.707536179	9.346671124	5.384543102
			0.5	1.160159942	0.937705250	9.265662314	1.997594676
			1.0	2.150493777	1.707536205	9.346671237	2.106243364
			1.5	3.087013054	2.416943407	9.433920745	2.203222922

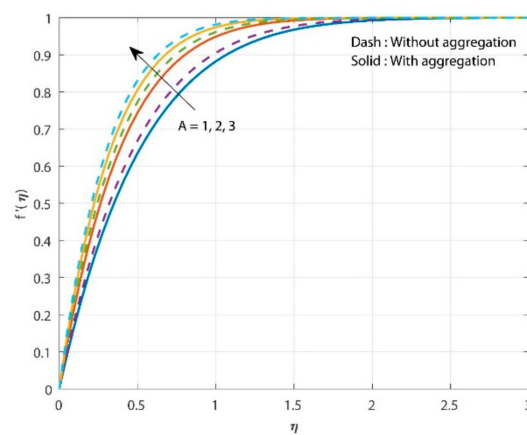


Figure 2. Influence of acceleration parameter on f' .

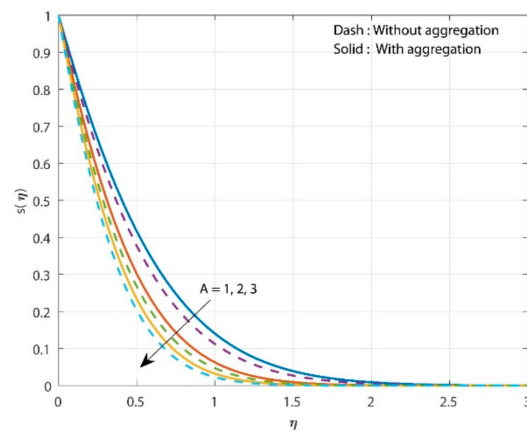


Figure 3. Influence of acceleration parameter on s .

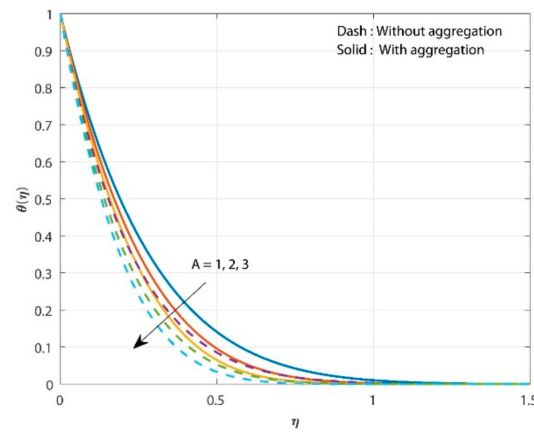


Figure 4. Influence of acceleration parameter on θ .

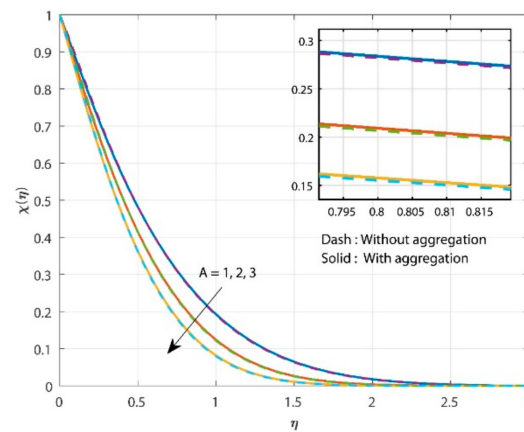


Figure 5. Influence of acceleration parameter on χ .

The variation in the rotational parameter (λ) on the primary velocity f' profile is shown in Figure 6. The increase in λ will accelerate the primary velocity f' . This is due to the rise in the λ , which includes additional momentum to the boundary layer, which results in a decline in the thickness of the boundary layer, causing the fluid to accelerate. It is also observed that nanoparticles without aggregation have lower velocity than nanoparticles with aggregation.

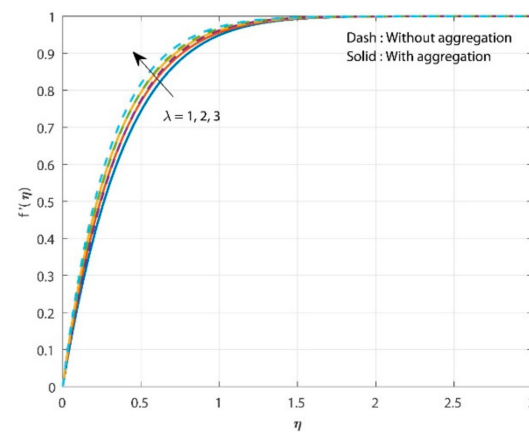


Figure 6. Influence of rotation parameter on f' .

The impact of the Schmidt number (Sc) and thermophoretic parameter (τ_1) on the concentration profile χ is illustrated in Figures 7 and 8. In the fluid flow, the ratio between mass and momentum diffusivity is called the Schmidt number. As the values of Sc decrease, the molecular diffusion results in a decrease in the concentration profile. A similar observation is noted in the case of τ_1 (see Figure 8). As τ_1 increases, it results in an increase in the temperature gradient, which leads to the motion of the nanoparticles from the hot to cold region. The nanoparticles without aggregation show greater concentration than nanoparticles with aggregation.

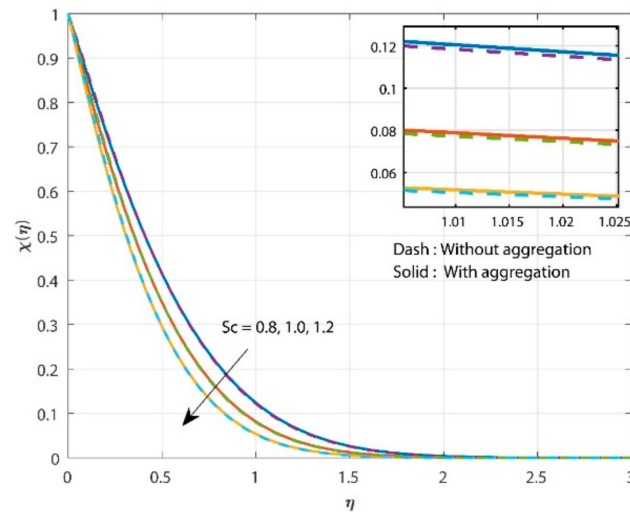


Figure 7. Influence of Schmidt number on χ .

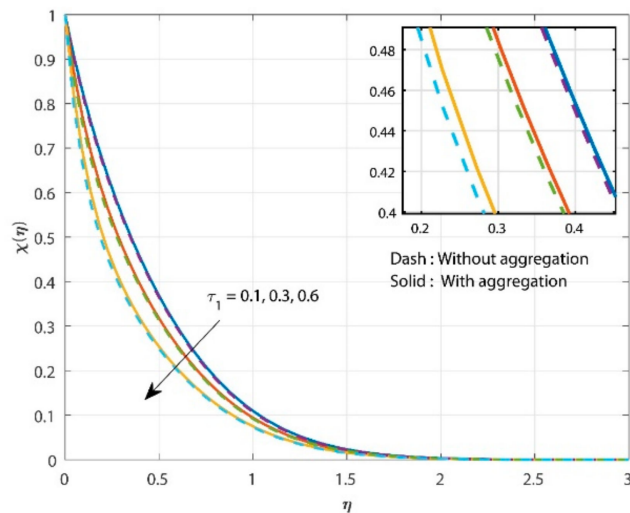


Figure 8. Influence of thermophoretic parameter on χ .

Figures 9 and 10 show the influence of λ on C_{fx} and C_{fz} for a variation in A . From the figure, it is observed that the surface drag force is enhanced with an improvement in the values of λ and A . A rise in the values of A and λ will decrease the thickness of the boundary layer, resulting in a high surface drag force. Surface drag force is greater in nanoparticles with aggregation than nanoparticles without aggregation in the C_{fx} case but the reverse trend is seen in the C_{fz} case.

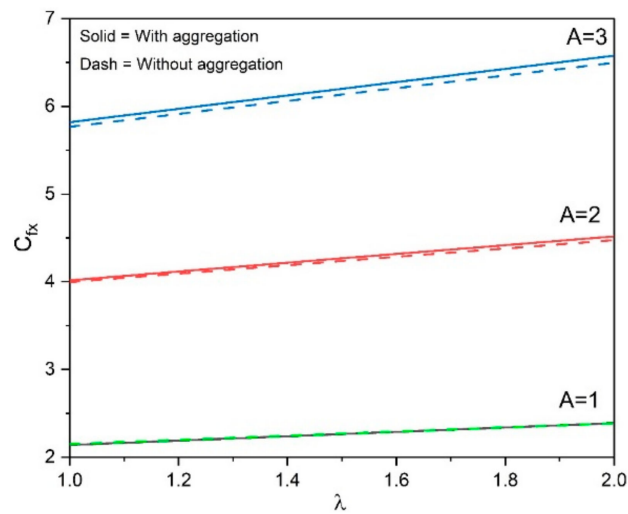


Figure 9. Influence of C_{fx} on λ for numerous values of A .

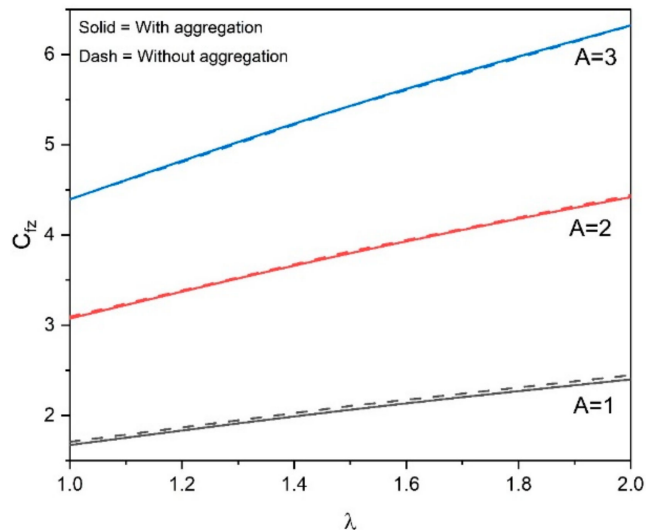


Figure 10. Influence of C_{fz} on λ for numerous values of A .

Figure 11 shows the variation in ϕ on Nu for numerous values of A . The rate of thermal distribution enhances with inclined values of ϕ . As the values of the rotational parameter and solid volume fraction rise, the Nu decreases; this is due to a decrease in the thickness due to the presence of A . It is clearly seen from the plot that nanoparticles without aggregation exhibit a higher rate of heat transfer than nanoparticles with aggregation. The rate of mass transfer on τ_1 for numerous values of A is illustrated in Figure 12. The growth in the values of τ_1 and A will increase the rate of mass transfer. The rate of mass transfer is greater in the case of nanoparticles without aggregation than nanoparticles with aggregation.

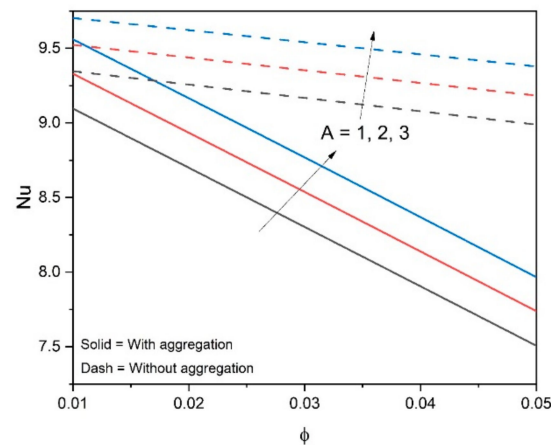


Figure 11. Influence of Nu on ϕ for numerous values of A .

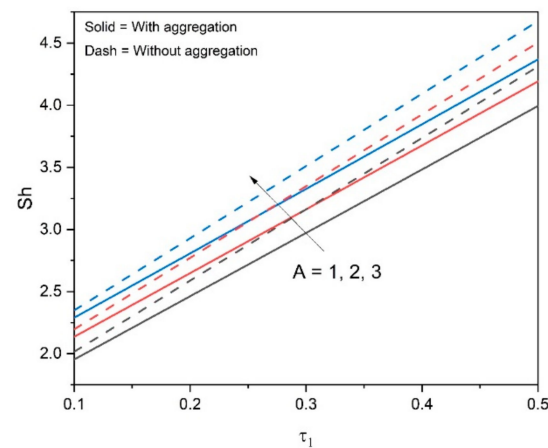


Figure 12. Influence of Sh on τ_1 for numerous values of A .

5. Conclusions

The current study is designed to examine the behavior of nanoparticle aggregation stagnation point flow over a rotating sphere with the occurrence of T-P-D. The numerical solutions to the flow governing equations are obtained with the help of the RKF-45 scheme by using the bvp5c package. The numerical data are graphically presented to show how the various dimensionless parameters fluctuate in their corresponding profiles. The following are the findings of the current investigation:

1. Primary velocity enhances with increasing values of the acceleration parameter, but secondary velocity diminishes;
2. Thermal distribution enhances in the case of nanoparticles in the absence of aggregation as compared to nanoparticles in the presence of aggregation over the acceleration parameter;
3. Growth in the rotational parameter will escalate the primary velocity;
4. For an inclination in the thermophoretic parameter, the concentration decreases more in the case of nanoparticle aggregation than in the absence of nanoparticle aggregation;
5. The surface drag force is greater in nanoparticles with aggregation than nanoparticles without aggregation in the C_{fx} case but the reverse trend is seen in the C_{fz} case;
6. The rate of heat distribution increases as the solid volume fraction rises, whereas the rate of mass transfer grows as the thermophoretic parameter increases.

The current work was limited to examining the behavior of nanoparticle aggregation stagnation point flow over a rotating sphere with the occurrence of thermophoretic particle

deposition. The current study may be expanded to investigate shape factor behavior in heat and mass transfer in the presence of ternary nanofluid flow.

Author Contributions: Conceptualization, J.K.M., B.C.P. and U.K.; methodology, S.M. and J.K.M.; software, S.M., J.K.M. and U.K.; validation, S.M., J.K.M., U.K. and B.C.P.; formal analysis, B.C.P. and A.M.G.; investigation, A.M.G., S.M. and B.C.P.; resources, A.M.G.; data curation, J.K.M.; writing—original draft preparation, S.M., U.K., J.K.M. and B.C.P.; writing—review and editing, Z.R., A.M.G. and S.M.; visualization, U.K., J.K.M., Z.R. and B.C.P.; supervision, Z.R.; project administration, Z.R. and A.M.G.; funding acquisition, Z.R. and A.M.G. All authors have read and agreed to the published version of the manuscript.

Funding: The authors extend their appreciation to the Deanship of Scientific Research at King Khalid University, Abha, Saudi Arabia, for funding this work through the Research Group Project under Grant Number (RGP.2/54/43).

Data Availability Statement: Not applicable.

Acknowledgments: The author (Z. Raizah) extends their appreciation to the Deanship of Scientific Research at King Khalid University, Abha, Saudi Arabia, for funding this work through the Research Group Project under Grant Number (RGP.2/54/43). We would like to thank the experts for their thoughtful comments and efforts toward improving our paper.

Conflicts of Interest: The authors declare no conflict of interest.

References

- Choi, S.U.S.; Eastman, J.A. *Enhancing Thermal Conductivity of Fluids with Nanoparticles*; Argonne National Lab. (ANL): Argonne, IL, USA, 1995.
- Abu-Nab, A.K.; Selima, E.S.; Morad, A.M. Theoretical investigation of a single vapor bubble during $\text{Al}_2\text{O}_3/\text{H}_2\text{O}$ nanofluids in power-law fluid affected by a variable surface tension. *Phys. Scr.* **2021**, *96*, 035222. [\[CrossRef\]](#)
- Prasannakumara, B.C. Assessment of the local thermal non-equilibrium condition for nanofluid flow through porous media: A comparative analysis. *Indian J. Phys.* **2021**, 1–9. [\[CrossRef\]](#)
- Khan, U.; Ahmad, S.; Hayyat, A.; Khan, I.; Nisar, K.S.; Baleanu, D. On the Cattaneo–Christov Heat Flux Model and OHAM Analysis for Three Different Types of Nanofluids. *Appl. Sci.* **2020**, *10*, 886. [\[CrossRef\]](#)
- Alzahrani, H.A.H.; Alsaiari, A.; Madhukesh, J.K.; Naveen Kumar, R.; Prasanna, B.M. Effect of thermal radiation on heat transfer in plane wall jet flow of Casson nanofluid with suction subject to a slip boundary condition. *Waves Random Complex Media* **2022**, 1–18. [\[CrossRef\]](#)
- Morad, A.M.; Selima, E.S.; Abu-Nab, A.K. Thermophysical bubble dynamics in N-dimensional $\text{Al}_2\text{O}_3/\text{H}_2\text{O}$ nanofluid between two-phase turbulent flow. *Case Stud. Therm. Eng.* **2021**, *28*, 101527. [\[CrossRef\]](#)
- Bhowmik, P.K.; Shamim, J.A.; Chen, X.; Suh, K.Y. Rod bundle thermal-hydraulics experiment with water and water- Al_2O_3 nanofluid for small modular reactor. *Ann. Nucl. Energy* **2021**, *150*, 107870. [\[CrossRef\]](#)
- Ahmed, F.; Abir, M.A.; Bhowmik, P.K.; Deshpande, V.; Mollah, A.S.; Kumar, D.; Alam, S. Computational assessment of thermo-hydraulic performance of Al_2O_3 -water nanofluid in hexagonal rod-bundles subchannel. *Prog. Nucl. Energy* **2021**, *135*, 103700. [\[CrossRef\]](#)
- Wensel, J.; Wright, B.; Thomas, D.; Douglas, W.; Mannhalter, B.; Cross, W.; Hong, H.; Kellar, J.; Smith, P.; Roy, W. Enhanced thermal conductivity by aggregation in heat transfer nanofluids containing metal oxide nanoparticles and carbon nanotubes. *Appl. Phys. Lett.* **2008**, *92*, 023110. [\[CrossRef\]](#)
- Xie, H.; Wang, J.; Xi, T.; Liu, Y.; Ai, F.; Wu, Q. Thermal conductivity enhancement of suspensions containing nanosized alumina particles. *J. Appl. Phys.* **2002**, *91*, 4568–4572. [\[CrossRef\]](#)
- Swain, K.; Mahanthesh, B. Thermal Enhancement of Radiating Magneto-Nanoliquid with Nanoparticles Aggregation and Joule Heating: A Three-Dimensional Flow. *Arab. J. Sci. Eng.* **2021**, *46*, 5865–5873. [\[CrossRef\]](#)
- Rana, P.; Mackolil, J.; Mahanthesh, B.; Muhammad, T. Cattaneo–Christov Theory to model heat flux effect on nanoliquid slip flow over a spinning disk with nanoparticle aggregation and Hall current. *Waves Random Complex Media* **2022**, 1–23. [\[CrossRef\]](#)
- Sabu, A.; Mackolil, J.; Mahanthesh, B.; Mathew, A. Nanoparticle aggregation kinematics on the quadratic convective magnetohydrodynamic flow of nanomaterial past an inclined flat plate with sensitivity analysis. *Proc. Inst. Mech. Eng. Part E J. Process Mech. Eng.* **2021**, *236*, 1056–1066. [\[CrossRef\]](#)
- Yu, Y.; Madhukesh, J.K.; Khan, U.; Zaib, A.; Abdel-Aty, A.-H.; Yahia, I.S.; Alqahtani, M.S.; Wang, F.; Galal, A.M. Nanoparticle Aggregation and Thermophoretic Particle Deposition Process in the Flow of Micropolar Nanofluid over a Stretching Sheet. *Nanomaterials* **2022**, *12*, 977. [\[CrossRef\]](#)
- Jestine, S.; Mahanthesh, B. Radiative heat transport and unsteady flow in an irregular channel with aggregation kinematics of nanofluid. *Heat Transf.* **2022**, *51*, 223–238. [\[CrossRef\]](#)

16. Wang, F.; Kumar, R.N.; Prasannakumara, B.C.; Khan, U.; Zaib, A.; Abdel-Aty, A.-H.; Yahia, I.S.; Alqahtani, M.S.; Galal, A.M. Aspects of Uniform Horizontal Magnetic Field and Nanoparticle Aggregation in the Flow of Nanofluid with Melting Heat Transfer. *Nanomaterials* **2022**, *12*, 1000. [[CrossRef](#)]
17. Green, H.L.; Lane, W.R. Particulate Clouds: Dusts, Smokes and Mists. Their Physics and Physical Chemistry and Industrial and Environmental Aspects. In *Particulate Clouds: Dusts, Smokes and Mists. Their Physics and Physical Chemistry and Industrial and Environmental Aspects*; E. & F. N. Spon, Ltd.: London, UK, 1957.
18. Fuchs, N.A. *The Mechanics of Aerosols*; Pergamon Press: Oxford, UK, 1964.
19. Goren, S.L. Thermophoresis of aerosol particles in the laminar boundary layer on a flat plate. *J. Colloid Interface Sci.* **1977**, *61*, 77–85. [[CrossRef](#)]
20. Madhukesh, J.K.; Alhadhrami, A.; Naveen Kumar, R.; Punith Gowda, R.J.; Prasannakumara, B.C.; Varun Kumar, R.S. Physical insights into the heat and mass transfer in Casson hybrid nanofluid flow induced by a Riga plate with thermophoretic particle deposition. *Proc. Inst. Mech. Eng. Part E J. Process Mech. Eng.* **2021**, 09544089211039305. [[CrossRef](#)]
21. Waini, I.; Khan, U.; Zaib, A.; Ishak, A.; Pop, I. Thermophoresis particle deposition of $\text{CoFe}_2\text{O}_4\text{-TiO}_2$ hybrid nanoparticles on micropolar flow through a moving flat plate with viscous dissipation effects. *Int. J. Numer. Methods Heat Fluid Flow* **2022**. [[CrossRef](#)]
22. Shankaralingappa, B.M.; Madhukesh, J.K.; Sarris, I.E.; Gireesha, B.J.; Prasannakumara, B.C. Influence of Thermophoretic Particle Deposition on the 3D Flow of Sodium Alginate-Based Casson Nanofluid over a Stretching Sheet. *Micromachines* **2021**, *12*, 1474. [[CrossRef](#)]
23. Chen, S.B.; Shahmir, N.; Ramzan, M.; Sun, Y.L.; Aly, A.A.; Malik, M.Y. Thermophoretic particle deposition in the flow of dual stratified Casson fluid with magnetic dipole and generalized Fourier's and Fick's laws. *Case Stud. Therm. Eng.* **2021**, *26*, 101186. [[CrossRef](#)]
24. Madhukesh, J.K.; Ramesh, G.K.; Alsulami, M.D.; Prasannakumara, B.C. Characteristic of thermophoretic effect and convective thermal conditions on flow of hybrid nanofluid over a moving thin needle. *Waves Random Complex Media* **2021**, 1–23. [[CrossRef](#)]
25. Punith Gowda, R.J.; Baskonus, H.M.; Naveen Kumar, R.; Prakasha, D.G.; Prasannakumara, B.C. Evaluation of heat and mass transfer in ferromagnetic fluid flow over a stretching sheet with combined effects of thermophoretic particle deposition and magnetic dipole. *Waves Random Complex Media* **2021**, 1–19. [[CrossRef](#)]
26. Zaib, A.; Khan, U.; Khan, I.; Seikh, A.H.; Sherif, E.-S.M. Entropy Generation and Dual Solutions in Mixed Convection Stagnation Point Flow of Micropolar Ti6Al4V Nanoparticle along a Riga Surface. *Processes* **2020**, *8*, 14. [[CrossRef](#)]
27. Khan, U.; Zaib, A.; Abu Bakar, S.; Ishak, A. Stagnation-point flow of a hybrid nanoliquid over a non-isothermal stretching/shrinking sheet with characteristics of inertial and microstructure. *Case Stud. Therm. Eng.* **2021**, *26*, 101150. [[CrossRef](#)]
28. Gul, T.; Ali, B.; Alghamdi, W.; Nasir, S.; Saeed, A.; Kumam, P.; Mukhtar, S.; Kumam, W.; Jawad, M. Mixed convection stagnation point flow of the blood based hybrid nanofluid around a rotating sphere. *Sci. Rep.* **2021**, *11*, 7460. [[CrossRef](#)]
29. Ghasemi, S.E.; Hatami, M. Solar radiation effects on MHD stagnation point flow and heat transfer of a nanofluid over a stretching sheet. *Case Stud. Therm. Eng.* **2021**, *25*, 100898. [[CrossRef](#)]
30. Malvandi, A. The unsteady flow of a nanofluid in the stagnation point region of a time-dependent rotating sphere. *Therm. Sci.* **2015**, *19*, 1603–1612. [[CrossRef](#)]
31. Mahdy, A.; Chamkha, A.J.; Nabwey, H.A. Entropy analysis and unsteady MHD mixed convection stagnation-point flow of Casson nanofluid around a rotating sphere. *Alex. Eng. J.* **2020**, *59*, 1693–1703. [[CrossRef](#)]
32. Ahmed, S.E.; Rashed, Z.Z. Unsteady MHD Mixed Convection Flow with Slip of a Nanofluid in the Stagnation Region of an Impulsively Rotating Sphere with Effects of Thermal Radiation and Convective Boundary Conditions. *World J. Mech.* **2018**, *8*, 137–160. [[CrossRef](#)]
33. Mackolil, J.; Mahanthesh, B. Sensitivity analysis of Marangoni convection in $\text{TiO}_2\text{-EG}$ nanoliquid with nanoparticle aggregation and temperature-dependent surface tension. *J. Therm. Anal. Calorim.* **2021**, *143*, 2085–2098. [[CrossRef](#)]
34. Mahanthesh, B. Flow and heat transport of nanomaterial with quadratic radiative heat flux and aggregation kinematics of nanoparticles. *Int. Commun. Heat Mass Transf.* **2021**, *127*, 105521. [[CrossRef](#)]
35. Chen, J.; Zhao, C.Y.; Wang, B.X. Effect of nanoparticle aggregation on the thermal radiation properties of nanofluids: An experimental and theoretical study. *Int. J. Heat Mass Transf.* **2020**, *154*, 119690. [[CrossRef](#)]
36. Mahanthesh, B.; Thriveni, K. Nanoparticle aggregation effects on radiative heat transport of nanoliquid over a vertical cylinder with sensitivity analysis. *Appl. Math. Mech.* **2021**, *42*, 331–346. [[CrossRef](#)]
37. Anilkumar, D.; Roy, S. Self-similar solution of the unsteady mixed convection flow in the stagnation point region of a rotating sphere. *Heat Mass Transf.* **2004**, *40*, 487–493. [[CrossRef](#)]